Supporting Information

Catalytic and photoresponsive BiZ/Cu$_x$S heterojunctions with surface vacancies for the treatment of multidrug-resistant clinical biofilm-associated infections

Amit Nain,[a,b,c,d] Hao-Hsin Huang,[e] Dan M Chevrier,[f] Yu-Ting Tseng,[g] Arumugam Sangili,[g] Yu-Feng Lin,[g] Yu-Fen Huang,[h] Lung Chang,*[i] Fu-Chieh Chang,[j,k,l] Chih-Ching Huang,[e,m] Fan-Gang Tseng,*[d,n,o] and Huan-Tsung Chang*[g]

[a]*Institute of Physics, Academia Sinica, Taipei 11529, Taiwan*

[b]*Nano Science and Technology Program, Taiwan International Graduate Program,*

[c]*Institute of Physics, Academia Sinica, Taipei 11529, Taiwan*

[d]*Department of Engineering and System Science, National Tsing Hua University, Hsinchu 30013, Taiwan*

[e]*Department of Bioscience and Biotechnology, National Taiwan Ocean University, Keelung 20224, Taiwan*

[f]*Biosciences and Biotechnologies Institute of Aix-Marseille (BIAM), CEA Cadarache, Bâtiment 1900, Saint-Paul-lez-Durance, France*

[g]*Department of Chemistry, National Taiwan University, Taipei 10617, Taiwan*

[h]*Institute of Analytical and Environmental Sciences, National Tsing Hua University, Hsinchu 30013, Taiwan*

[i]*Department of Pediatrics, Mackay Memorial Hospital and Mackay Junior College of*

[j]*Infection Control Centre, Mackay Memorial Hospital, Taipei, 10449, Taiwan*

[k]*College of Management, Yuan Ze University, Taoyuan City, 32003, Taiwan*

[l]*Nursing and Management, Mackay Junior College of Medicine, Taipei, 10650, Taiwan*

[m]*Centre of Excellence for the Oceans, National Taiwan Ocean University, Keelung 20224, Taiwan*

[n]*Research Centre for Applied Sciences Academia Sinica, Taipei 11529, Taiwan*

[o]*Frontier Research Centre on Fundamental and Applied Sciences of Matters, National Tsing Hua University, Hsinchu 30013, Taiwan*

Table of Contents

Supplementary experimental section

Materials

Bismuth nitrate pentahydrate (Bi(NO$_3$)$_3$·5H$_2$O), nitric acid (HNO$_3$, 65%), crystal violet dye, and bovine serum albumin (BSA) were obtained from Sigma–Aldrich (St. Louis, MO, USA). Copper sulfate anhydrous (CuSO$_4$) was purchased from Kanto Chemical (Tokyo, Japan). Sodium phosphate monobasic monohydrate (NaH$_2$PO$_4$·H$_2$O), sodium phosphate dibasic heptahydrate (Na$_2$HPO$_4$·7H$_2$O), and sodium sulfide non-hydrate (Na$_2$S·9H$_2$O) were acquired from Acros Organics (Geel, Belgium). 10–Acetyl–3,7–dihydroxyphenoxazine (Amplex Red) was obtained from Invitrogen (Carlsbad, CA, USA). Hydrogen peroxide (aqueous solution, 35%) was purchased from Showa Chemical Industries Co. Ltd., Tokyo, Japan, respectively. Sodium hydroxide (NaOH) was bought from J.T. Baker (Center Valley, PA, USA). Bacterial strains [*S. aureus* (BCRC10781), *S. enteritidis* (BRBC 10744), *E. coli* (BRBC 12438), *P. aeruginosa* (ATCC 27853), and MRSA (methicillin–resistant *Staphylococcus aureus* (ATCC 43300)] were procured from the Institute of Food Science (Hsinchu, Taiwan). Milli–Q ultrapure water (18.2 MΩ cm) from Millipore (Billerica, MA, USA) was used in all experiments.

Characterization of BSA–BiZ/Cu$_x$S, –Cu$_x$S, and –Bi$_2$S$_3$ nanomaterials

Solutions were purified using centrifugation (3 washing cycles) to remove unreacted metal ions (Cu^{2+} and Bi^{3+}), free BSA, and excess NaOH. Final concentrations of Cu and Bi in BSA–BiZ/Cu$_x$S NCs, BSA–Cu$_x$S NPs, and BSA–Bi$_2$S$_3$ NPs separately dissolved in 2.0 % HNO$_3$ solution were determined by inductively coupled plasma mass spectrometry (ICP–MS; Agilent 7700 Series, Agilent Technologies, Santa Clara, CA, USA). The X-ray source (SP12B1; energy range: 8–25 KeV) from a bending magnet was used to record the diffraction patterns for BSA–BiZ/Cu$_x$S NCs, BSA–Cu$_x$S NPs, and BSA–Bi$_2$S$_3$ NPs, which were recorded using a CCD detector (BL12B2, Spring–8, and a 3–pin plate diamond anvil cell) from Almax easyLab (Almax Industries, Diksmuide, Belgium). The two–dimensional images were then integrated using the FIT2D proGram, with "Appendix" to set the wavelength corresponding to Cu Kα (1.5418 Å). High–resolution transmission electron microscopy (HR–TEM) images of BSA–BiZ/Cu$_x$S NCs, BSA–Cu$_x$S NPs, and BSA–Bi$_2$S$_3$ NPs were captured using field emission transmission electron microscopy (FE–TEM) equipped with dual focused ion beam system (FIB) and energy

dispersive X–ray spectrometer (EDS). UV–Vis absorption spectra of the BSA–BiZ/Cu$_x$S NCs, BSA–Cu$_x$S NPs, and BSA–Bi$_2$S$_3$ NPs in the range of 200–1400 nm was measured using a double–beam Jasco UV/VIS/NIR spectrophotometer (V–570, Easton, MD, USA). Each of the solution was diluted 10,000-fold in DI water, from which 2.0 μL was doped onto a carbon–coated grid and vacuum dried for 48 h at room temperature before measurements. The binding energies of the elements C, O, Cu, Bi, and S were obtained from X-ray photoelectron spectroscopy (XPS, VG ESCA210) from VG Scientific (West Sussex, UK). All the binding energies were corrected using C 1s (284.6 eV) as an internal standard. Aliquots (50 μL) of 10-fold concentrated BSA–BiZ/Cu$_x$S NCs and BSA–Cu$_x$S NPs solutions were simply dropped onto Si substrate and vacuum dried at room temperature for XPS analysis. Laser desorption/ionization time–of–flight mass spectrometry (LDI–TOF MS) was used to identify the possible components in BSA–BiZ/Cu$_x$S NCs and BSA–Cu$_x$S NPs using AutoflexIII S3 LDI–TOF MS (Bruker Daltonics, Bremen, Germany). Each of the sample was irradiated with a Nd:YAG pulse laser (355 nm, 100 Hz; 500 shots, pulse width: 6 ns, power density: 5 x 10^4 W cm^{-2}). Each of the MS signals was accumulated from five target positions. Fourier transform infrared (FTIR) spectroscopy analysis for BSA–BiZ/Cu$_x$S NCs and BSA–Cu$_x$S NPs were performed with Nicolet iS5 FTIR spectrometer (Thermo Scientific, Waltham, MA, USA). Their circular dichroism (CD) spectra in a cuvette of path length 1cm were recorded using J–815 spectrometers (JASCO, Tokyo, Japan) at room temperature.\

Bacterial viability assays

Bacterial suspensions of *E. coli* (1.0 × 10^8 CFU mL^{-1}) were incubated separately with BSA–BiZ/Cu$_x$S NCs ([Cu]= 0.2 μg mL^{-1}) and BSA–Cu$_x$S NPs ([Cu] = 0.2 μg mL^{-1}) dispersed in 10 mM sodium phosphate buffer (pH 7.4) for 10 min with and without NIR laser irradiation (808 nm, 0.53 W cm^{-2}) at room temperature. The untreated and treated bacterial samples were centrifuged (RCF 3000 × *g*, 5 min, 27 °C) and washed thrice with 10 mM sodium phosphate buffer (pH 7.4, 1.0 mL) prior to fluorescence assessment. A LIVE/DEAD BacLight Bacterial Viability Kit (Molecular Probes, Eugene, OR, USA) was used to quantify live/dead bacteria ratio in each of the tested sample. Typically, 1.0 μL of SYTO 9:PI (1:1) was added into each of the treated and untreated (negative control) bacterial samples, followed by incubation in the dark for 20 min at room temperature. Dye–suspensions were then centrifuged (RCF 3000 × g, 5 min, 27 °C) to remove the unbound dyes, and washed thrice with sodium phosphate buffer

(10 mM, pH 7.4). Aliquots (1.0 µL) of the purified solutions were dropped onto the glass slide for bright field and fluorescence microscopic analysis. The green and red fluorescence observed through emission filters of ≥525 nm, when excited with an Hg lamp with an excitation filter 460–490 nm (Olympus 1X71 microscope, Tokyo, Japan) represents the live and dead bacteria, respectively.

Reactive oxygen species (ROS) assays

Bacterial culture of *E. coli* (1.0×10^8 CFU mL^{-1}) were treated separately with 0.25 µg mL^{-1} (in terms of Cu) of BSA–BiZ/Cu$_x$S NCs and BSA–Cu$_x$S NPs dispersed in sodium phosphate buffer (10 mM, pH 7.4) in absence and presence of NIR laser (808 nm, 0.53 W cm^{-2}) at room temperature for 10 min. The untreated and hydrogen peroxide (H$_2$O$_2$; 10 mM)–treated bacteria culture served as the negative and positive controls, respectively. Each of the mixture was then centrifuged (RCF 3000 × *g*, 5 min, 27 °C) and washed thrice with 10 mM sodium phosphate buffer (pH 7.4). Subsequently, 2′,7′–Dichlorodihydrofluorescein diacetate (DCFH–DA, 100 µM) was separately added to each of the bacterial sample and incubated for 2 h at room temperature. Then, an aliquot (200 µL) of the solution from each vial was transferred into a 96–well flat–bottom microplate to measure the fluorescence intensities at an excitation/emission wavelengths of 490/530 nm, respectively, using a monochromatic microplate spectrophotometer.

Permeability of bacterium membrane

Bacterial suspensions of *E. coli* (1.0×10^8 CFU mL^{-1}) were incubated separately with BSA–BiZ/Cu$_x$S NCs ([Cu]=4.0 µg mL^{-1}) and BSA–Cu$_x$S NPs ([Cu] = 4.0 µg mL^{-1}), with and without NIR laser irradiation (808 nm, 0.53 W cm^{-2}) for 10 min at room temperature. PBS and B-PER lysis buffer treated aliquots were used as positive and negative control, respectively. Each of the solutions (1.0 mL) was centrifuged at an RCF of 3000 × g for 5 min. The supernatants were then incubated separately with 200 µM *o*-nitrophenyl-*β*-D-galactopyranoside (ONPG) at room temperature for 2 h with orbital shaking. Lastly, 200 µL of each solution was transferred in a 96-well flat-bottom microplate to record its absorbance at 420 nm by using a monochromatic microplate spectrophotometer (Synergy 4, Biotek Instruments, Winooski, VT, USA).

SEM and TEM images of bacteria

1.0 mL of bacteria suspension (*E. coli*; 1.0×10^8 CFU mL^{-1}) was centrifuged (RCF 3000 × g, 5 min, 27 °C) and then dispersed in 10 mM sodium phosphate buffer (pH 7.4, 1 mL). Bacterial culture (1×10^7 CFU mL^{-1}) of *E. coli* was untreated (negative control) and separately incubated with 4.0 µg mL^{-1} (in terms of Cu) of BSA–BiZ/Cu$_x$S NCs and BSA–Cu$_x$S NPs with and without NIR laser irradiation (808 nm, 0.53 W cm^{-2}) for 10 min at room temperature. The mixtures were then purified by centrifugation (RCF 3000 × g, 5 min, 27 °C) and washed with 10 mM sodium phosphate buffer (pH 7.4, 1.0 mL) before the pellets were suspended in 10 mM sodium phosphate buffer (pH 7.4, 1.0 mL). Then, the cells were fixed using 1.0 % glutaraldehyde at room temperature for 30 min. Afterwards, the bacteria solutions were centrifuged (RCF 3000 × g, 5 min, 27 °C) and redispersed in 10 mM sodium phosphate buffer (pH 7.4). Finally, 5 µL (1×10^5 CFU mL$^-$) from each of the resuspended solution was immobilized and vacuum dried (2 h, 27 °C) on a Si substrate and copper–coated carbon grid for SEM and TEM analysis, respectively.

In vitro cytotoxicity assays

The cytotoxicity of BSA–BiZ/Cu$_x$S NCs and BSA–Cu$_x$S NPs were investigated using Alamar blue assay (Thermo Fisher Scientific Inc.). Briefly, HaCaT cells (aneuploid immortal keratinocyte cell line from adult human skin, ATCC, Manassas, VA, USA) were seeded in 96–well plates (1×10^4 cells/well) and cultured for 12 h at 37 °C in a humidified incubator. Various concentrations ([Cu] = 0–80 µg mL^{-1}) of BSA–BiZ/Cu$_x$S and BSA–Cu$_x$S NPs NCs were incubated separately with the cells for 24 h at 37 °C. The nanomaterials were then replaced with a fresh medium for further growth for 24 h at 37 °C. Afterwards, the culture media were removed and cells were incubated with the Alamar blue solution (100 µL, 1x in DMEM plus 10% FBS) at 37 °C for 2 h. The fluorescence intensity of each well was measured using a microplate reader at an excitation/emission wavelengths of 550/600 nm, respectively. The cell viability (%) was determined as per the following equation:

Cell viability (%) = (F_{Test}/ F_{Blank}) × 100%, where, F_{Test} and F_{Blank} are the fluorescence intensities of the cells in the presence and absence of nanomaterials.

Hemolysis assays

A blood sample was withdrawn from the vein of a 28–year–old healthy male and stored in a sterile test tube containing trisodium citrate ($Na_3C_6H_5O_7$). The red blood cell (RBCs) collection protocols employed were according to the university guidelines and relevant laws. The blood sample was promptly centrifuged (3000 × g, 10 min, 4 °C) to remove the serum, and washed three times with PBS solution (pH 7.4). Various amounts ([Cu] = 0–80 μg mL^{-1}) of BSA–Bi/Cu$_x$S NCs and BSA–Cu$_x$S NPs were incubated separately with RBCs (~ 4 vol.% of blood cells) containing PBS (pH 7.4) for 1 h at room temperature. The mixtures were centrifuged (RCF 3000 × g, 10 min, 4°C) and the supernatants were subjected to absorption measurement at 576 nm (Abs$_{576}$). RBCs treated separately with PBS (1x, pH 7.4) and DI water served as negative (0% hemolysis, Abs$_{576\ blank}$) and positive (100% hemolysis, Abs$_{576\ water}$) controls, respectively. The hemolysis (%) was determined using the following formula:

Hemolysis (%) = [(Abs$_{576\ Test}$ – Abs$_{576\ Blank}$) / (Abs$_{576\ Water}$ – Abs$_{576\ Blank}$)
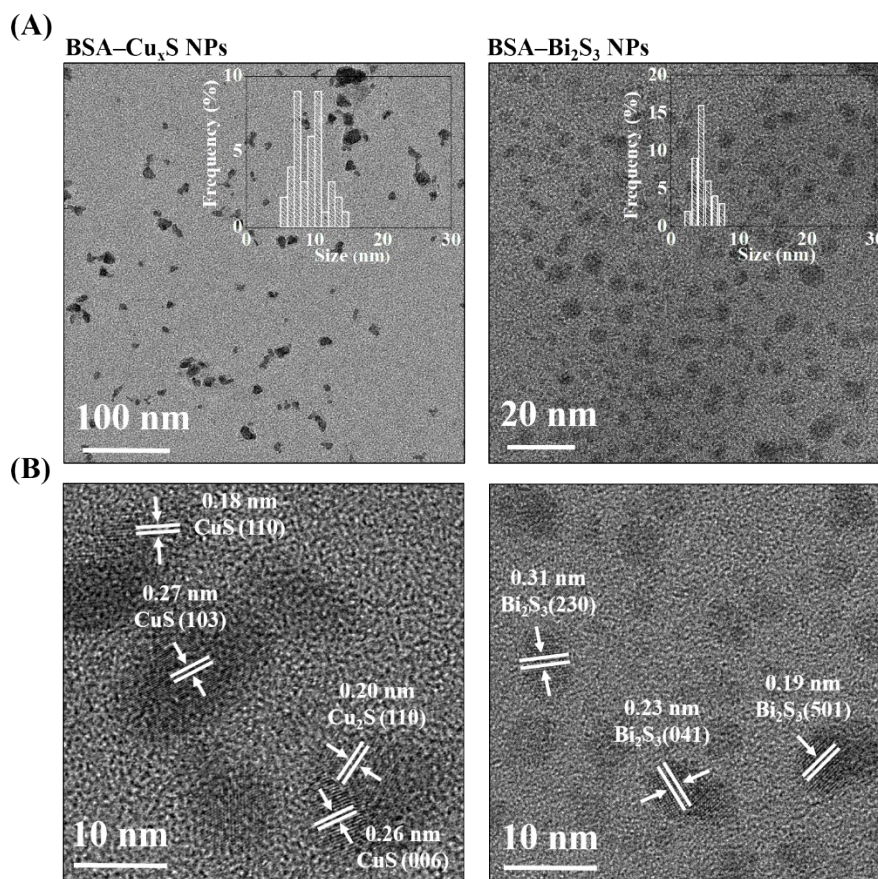
Fig. S1 (A) TEM and (B) corresponding HR-TEM images of BSA–Cu$_x$S NPs and BSA–Bi$_2$S$_3$ NPs. The insets to (A) show the particle size distribution.
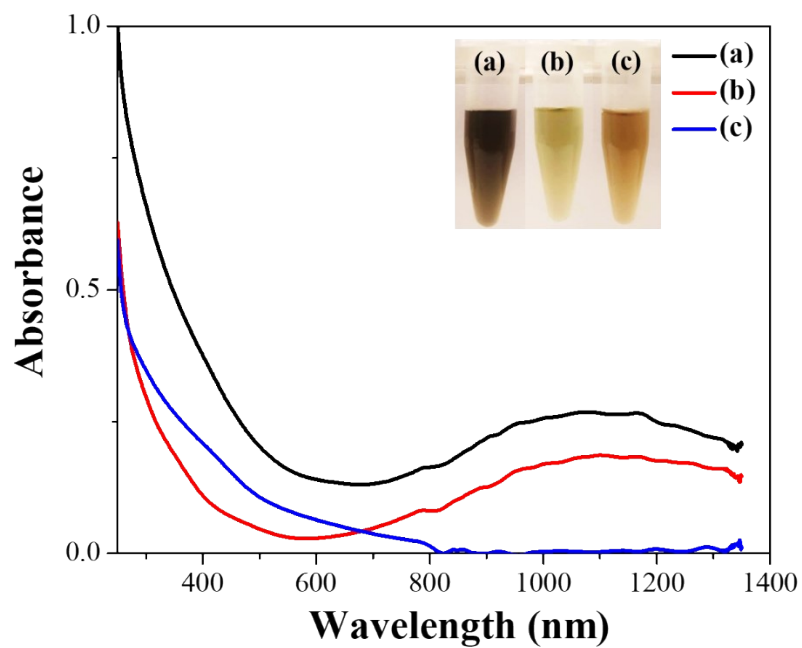
Fig. S2. UV-Vis-NIR absorption spectra of (a) BSA–BiZ/Cu$_x$S NCs (b) BSA–Cu$_x$S NPs, and (c) BSA–Bi$_2$S$_3$ NPs, with 20-fold dilution of as-prepared solutions in 10 mM sodium phosphate buffer (pH 7.4). Insets show the digital photographs of the corresponding solutions.
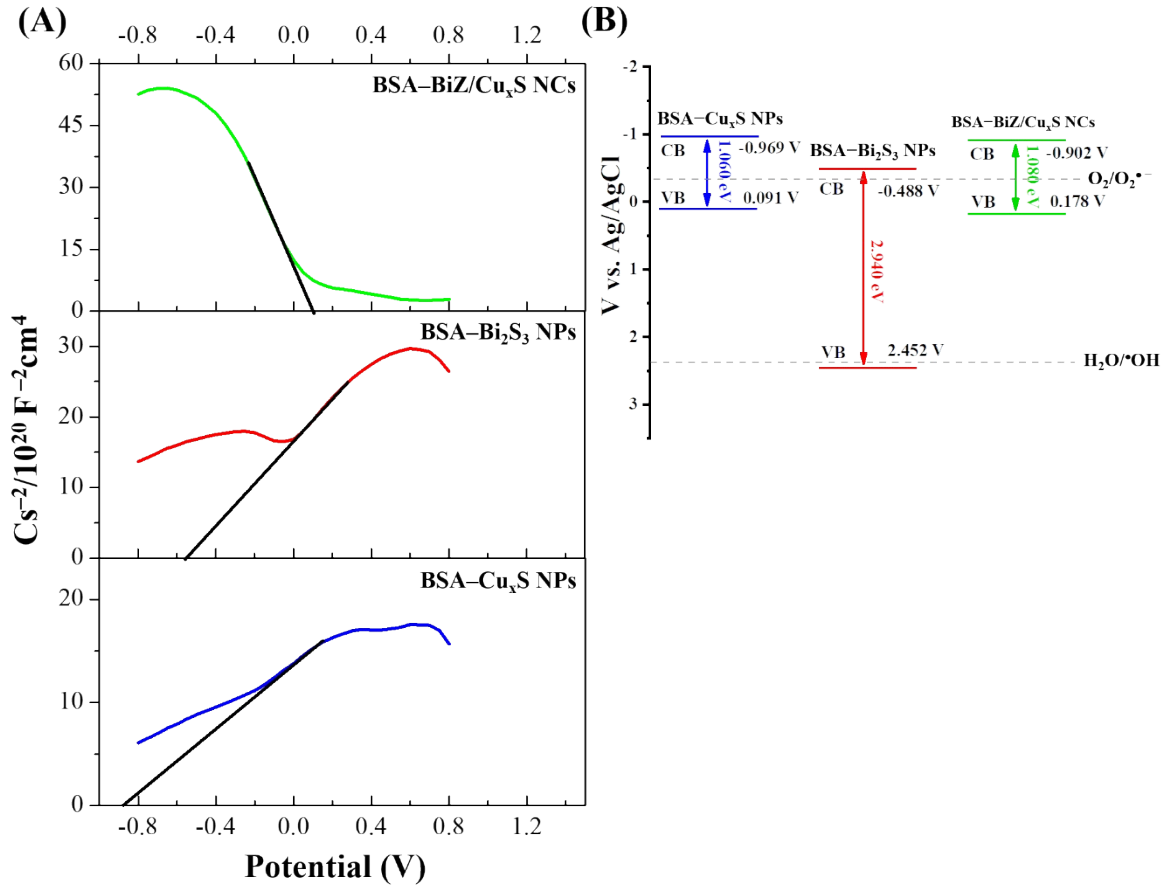
Fig. S3. (A) Mott–Schottky plots for the BSA–BiZ/Cu$_x$S NCs, BSA–Cu$_x$S NPs, and BSA–Bi$_2$S$_3$ NPs in 0.1 M sodium sulfate (Na$_2$SO$_4$). (B) Energy band diagram based on the determined flat band potential.

We use Mott-Schottky (M–S) plots to determine the position of the band edges of the BSA–BiZ/Cu$_x$S NCs, BSA–Cu$_x$S NPs, and BSA–Bi$_2$S$_3$ NPs. The carrier density (N_d) and flat band potential (V_{FB}) of the materials is calculated using the well-known M-S equation (1).[1]

$$\frac{1}{C^2} = \left(\frac{2}{N_d \varepsilon \varepsilon_0 e_0 A^2}\right) \times \left(V - V_{FB} - \frac{k_B T}{e_0}\right) \qquad (1)$$

where N_d is carrier donor density (cm^3), C is space charge capacitance, ε is the dielectric constant of nanomaterials, ε_0 the vacuum permittivity (8.85×10^{-14} F m^{-1}), A is working area of electrode (GCE; 0.0729 cm^2), V is applied potential, V_{FB} is flat–band potential, k_B is Boltzmann constant (1.38 × 10^{-23} m^2 kg s^{-2} K^{-1}), T is absolute temperature (K), and e_0 is the electric charge (1.60 × 10^{-19} C). The V_{FB} can be estimated from the x-intercept of the M–S plot (V versus 1/C^2). In contrast, the N_d of the semiconductor at the semiconductor-liquid interface is calculated from the corresponding slope (Δ) expressed in the following:

$$N_d = \left(\frac{2}{\varepsilon \varepsilon_0 e_0}\right) \times \Delta \qquad (2)$$

The value of V_{FB} given in equation (1) approximately refers to the valence band edge (V_{VB}) potentials and conduction band edge (V_{CB}) in the case of n and p-type semiconductors, respectively. Tauc plot shows the bandgap energies of the as-prepared BSA–Cu$_x$S NPs, BSA–Bi$_2$S$_3$ NPs, and BSA–BiZ/Cu$_x$S NCs are 1.060, 2.940, and 1.080 eV, respectively. The flat-band potential determined for BSA–BiZ/Cu$_x$S NCs (0.178 V) is positively shifted relative to BSA–Cu$_x$S NPs (−0.969 V) and BSA–Bi$_2$S$_3$ NPs (−0.488 V) in Na$_2$SO$_4$ solution. According to flat-band potentials calculated by M–S plots, the CB/VB positions of BSA–Cu$_x$S NPs, BSA–Bi$_2$S$_3$ NPs, and BSA–BiZ/Cu$_x$S NCs, were estimated to be −0.969/0.091, −0.488/2.452, and −0.902/0.178 eV eV, respectively.
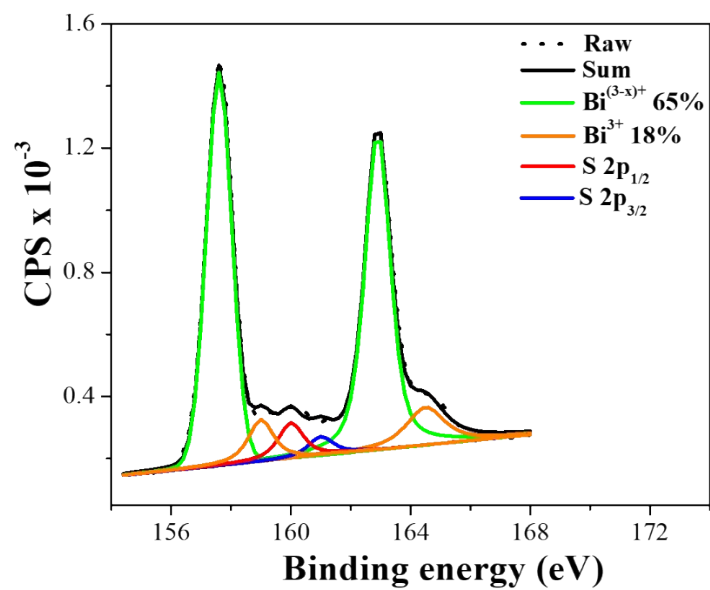
Fig. S4. Raw and deconvoluted Bi 4f and S 2p XPS spectra of BSA–Bi$_2$S$_3$ NPs.
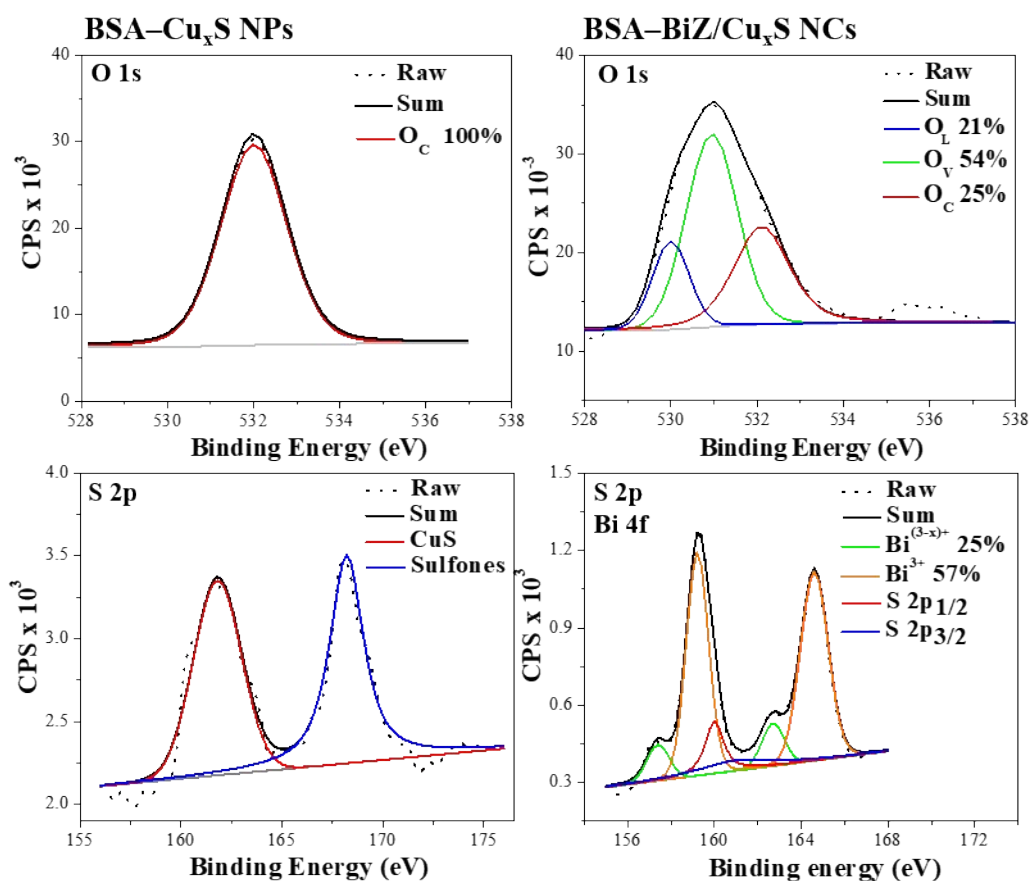
Fig. S5. Raw and deconvoluted XPS spectra of BSA–Cu$_x$S NPs and BSA–BiZ/Cu$_x$S NCs. The binding energies were corrected using C 1s (284.6 eV) as a standard. The lattice oxygen, chemisorbed or dissociated oxygen, oxygen vacancy, and defect are denoted as O$_L$, O$_C$, and O$_V$, respectively.
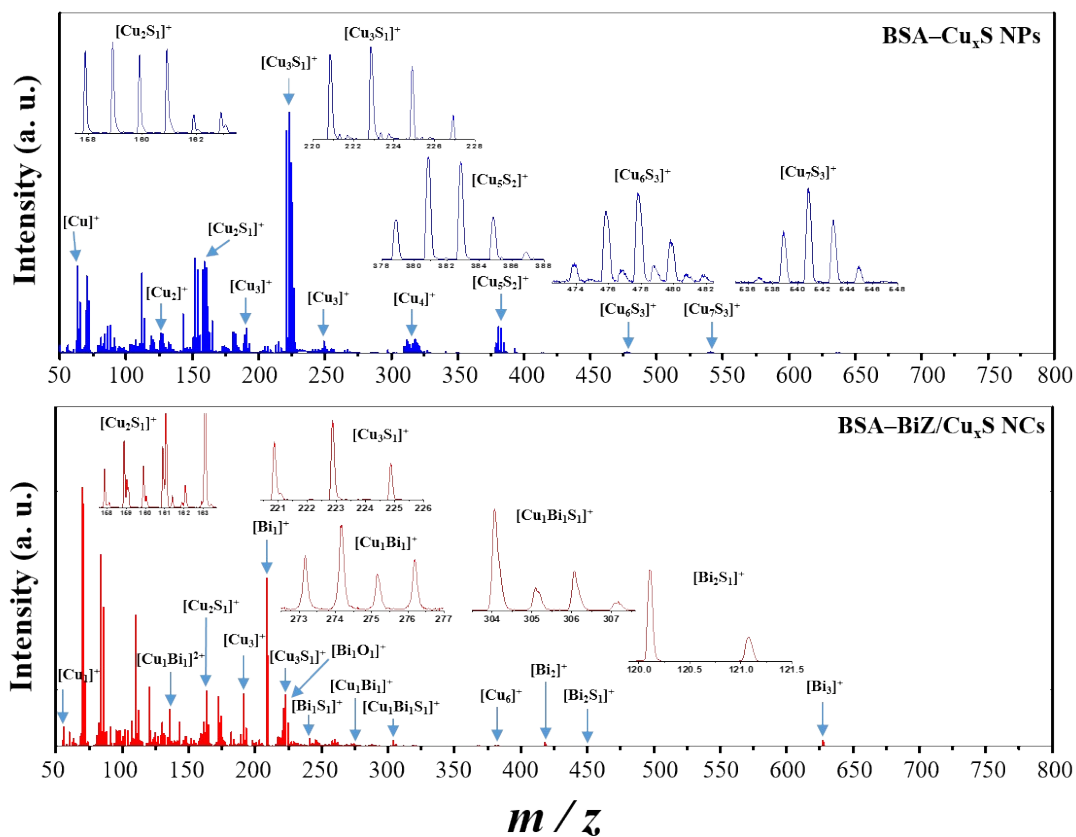
Fig. S6. LDI-MS spectra of BSA–BiZ/Cu$_x$S NCs and BSA–Cu$_x$S NPs. Insets show the theoretical isotope patterns. Peak intensities are plotted in arbitrary units (a. u.).
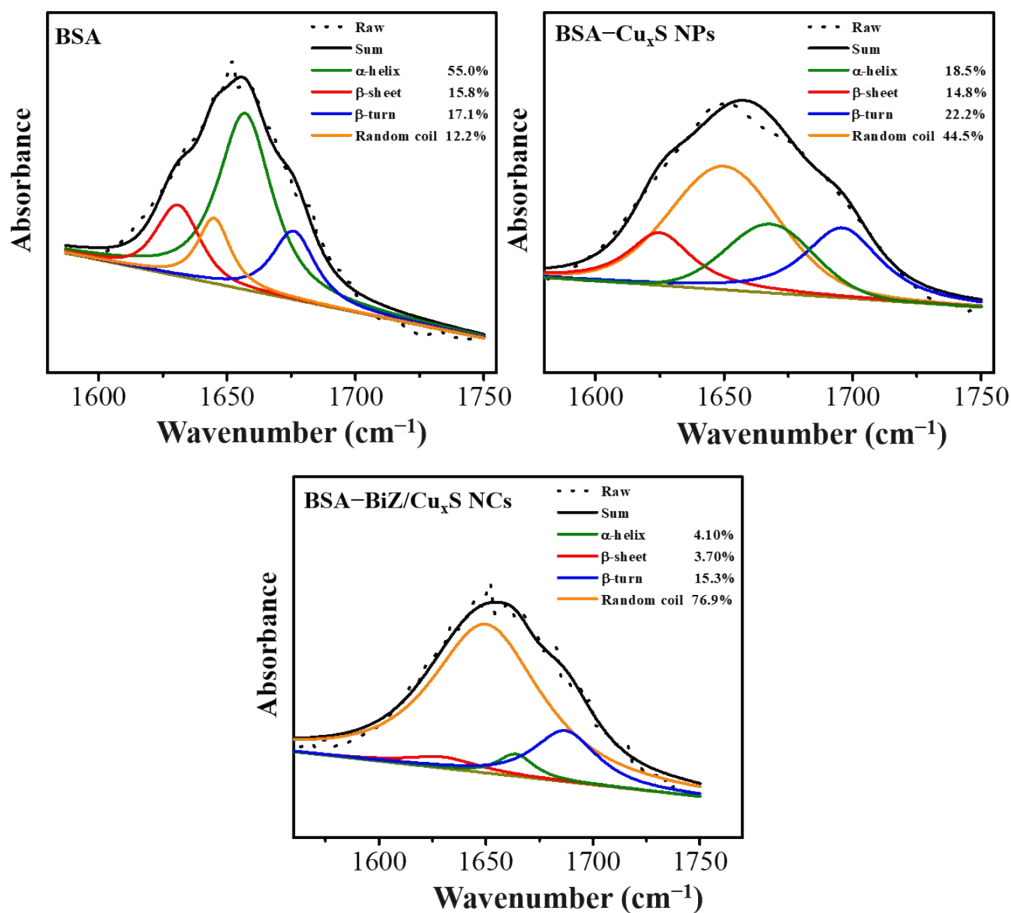
Fig. S7. Deconvoluted amide I band in the FT-IR spectra of BSA–BiZ/Cu$_x$S NCs, BSA–Cu$_x$S NPs, and free BSA. The concentration of BSA was the same (0.5 µM) in all four samples.

Deconvoluted FT-IR spectra of the amide I band (1600–1720 cm^{-1}) employed to study the compositions of α-helix (1643–1664 cm^{-1}), β-sheet (1615–1635 cm^{-1}), β-turn (1661–1687 cm^{-1}), and random coil (1632–1646 cm^{-1}). The deconvoluted amide I band displays much higher random coil structures in BSA–BiZ/Cu$_x$S NCs (76.9%) as compared to BSA–Cu$_x$S NPs (44.5%) and native BSA (12.2%), evidencing the higher partial denaturation of BSA after the formation of NCs in an alkaline solution.
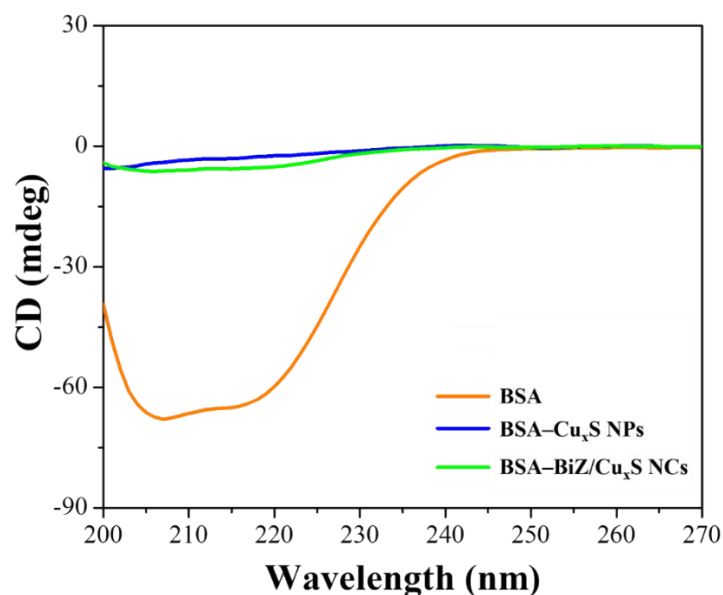
Fig. S8. CD spectra of BSA–BiZ/Cu$_x$S NCs, BSA–Cu$_x$S NPs, and free BSA dispersed in 10 mM sodium phosphate buffer (pH 7.4). The concentration of BSA was the same (0.5 µM) in all four samples. The percentage compositions of α-helix/ß-strands/random coil in the BSA–BiZ/Cu$_x$S NCs, BSA–Cu$_x$S NPs, and BSA analyzed by using K2D3 software available at http://k2d3.ogic.ca are 5%/19%/76%, 20%/36%/44%, and 57%/32%/11%, respectively.

The CD spectra of native BSA revealed the presence of α-helix (57%), ß-strands (32%), and random coil (11%) structures are consistent with the FT-IR measurements. The secondary structures of BSA in the BSA–BiZ/Cu$_x$S NCs and BSA–Cu$_x$S NPs were faded to 5−20%, whereas the random coil structures increased to 44−76%, further corroborating the fact that BSA acted as a stabilizer/template to stabilize the nanomaterials.
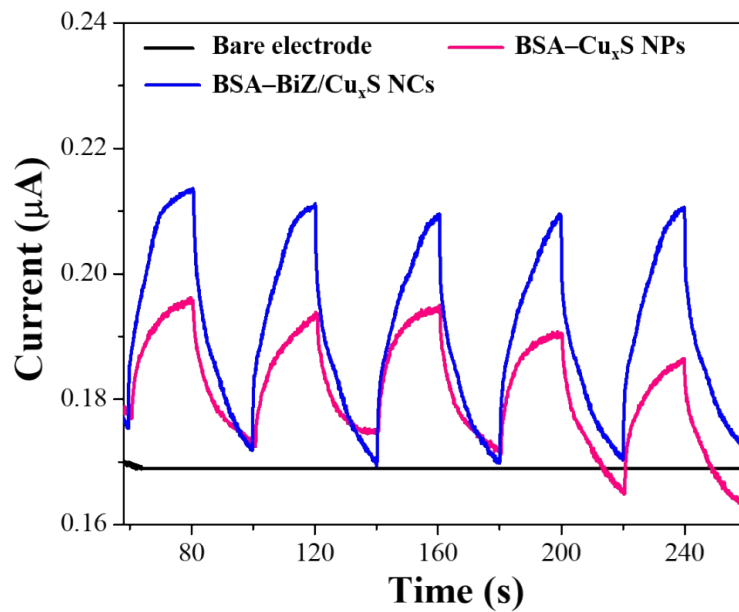
Fig. S9. Photocurrent response profile of BSA–BiZ/Cu$_x$S NCs and BSA–Cu$_x$S NPs in sodium sulfate solution (Na$_2$SO$_4$, 0.1 M) under white LED irradiation (0.31 W cm^{-2}) at 0.25 V. The 'on' and 'off' time interval is 20 s.
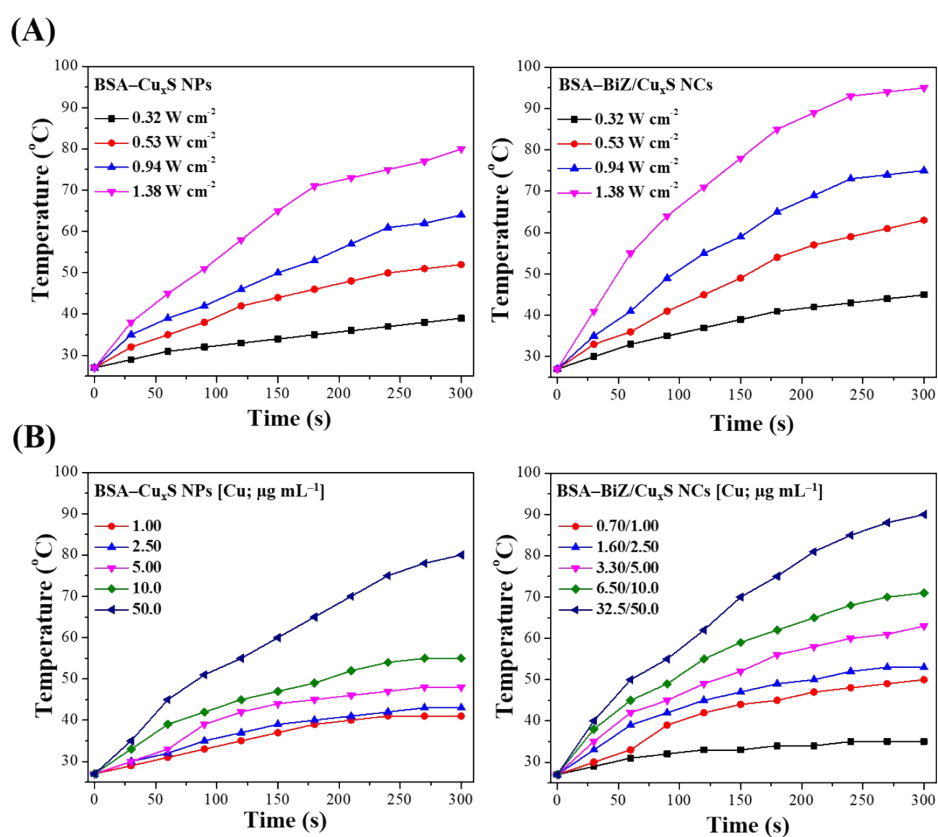
Fig. S10. (A) Power density- and (B) concentration-dependent temperature profile of BSA–BiZ/Cu$_x$S NCs and BSA–Cu$_x$S NPs in sodium phosphate buffer (10 mM, pH 7.4) solution. The concentration in (A) are 5.0 μg mL^{-1} (in terms of Cu) and power density of the 808 nm NIR laser in (B) is 0.53 W cm^{-2}.
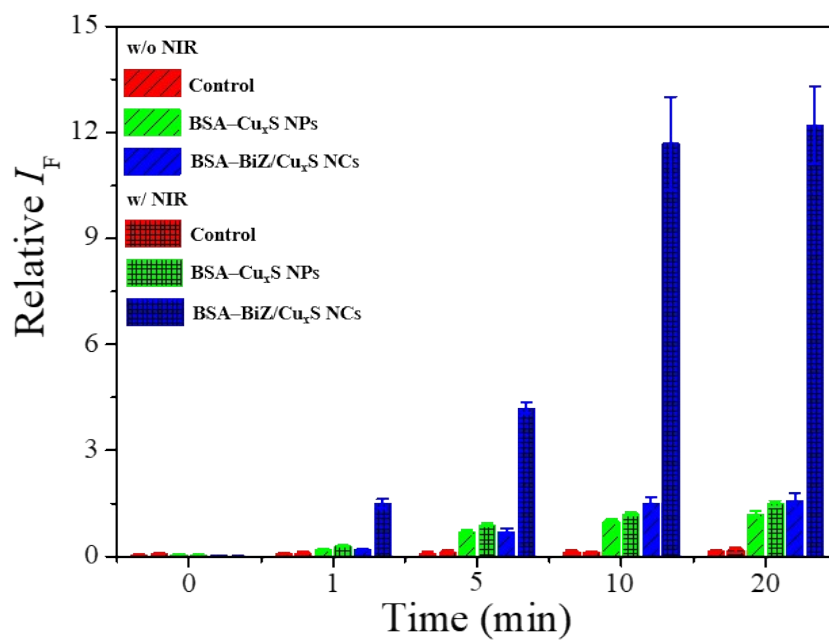
Fig. S11. Relative fluorescence intensity of AR (10 µM) incubated separately with BSA–Cu$_x$S NPs and BSA–BiZ/Cu$_x$S NCs in the absence and presence of NIR irradiation for 1, 5, and 10 min. The error bars represent standard deviations derived from four repeated experiments. The concentration of NCs or NPs is 5.0 µg mL^{-1} (in terms of Cu).
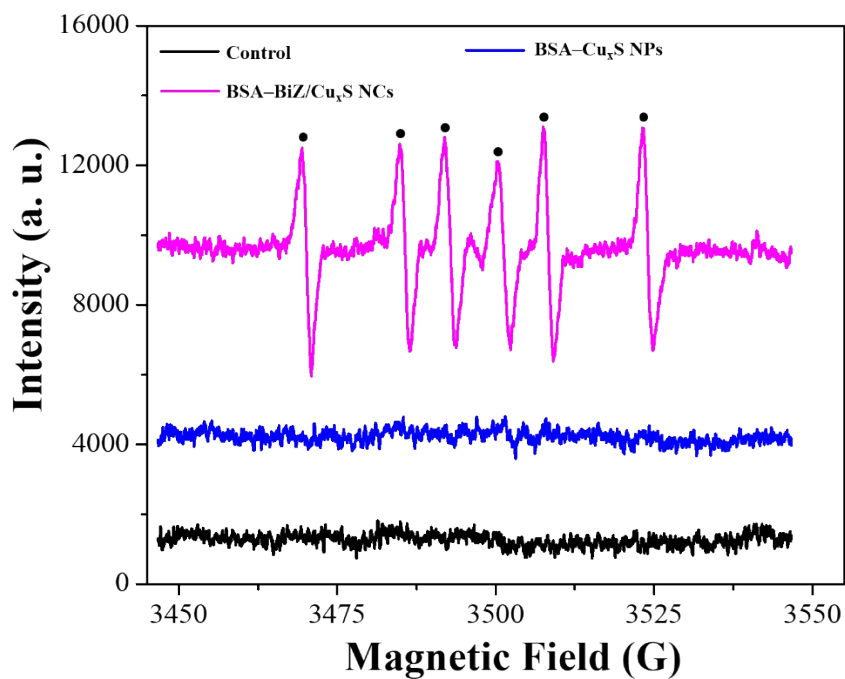
Fig. S12. ESR spectra of DMPO (10 mM) in sodium phosphate buffer (10 mM, pH 7.4) in the absence (as a control) and presence of 5.0 µg mL^{-1} (in terms of Cu) of BSA–BiZ/Cu$_x$S NCs and BSA–Cu$_x$S NPs without NIR laser irradiation. Black dots show the signal intensity from DMPO–·OOH adducts (a_N = 1.42 G a_H^β = 1.135 G).

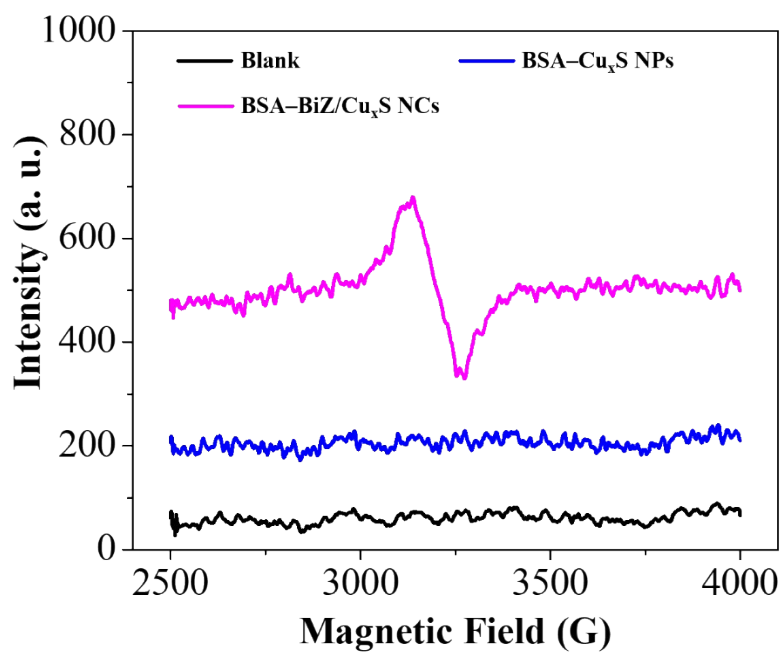**Fig. S13.** ESR spectra of in the absence (as a control) and presence of 5.0 µg mL^{-1} (in terms of Cu) of BSA–Bi/Cu$_x$S NCs and BSA–Cu$_x$S NPs dispersed in sodium phosphate buffer (10 mM, pH 7.4).
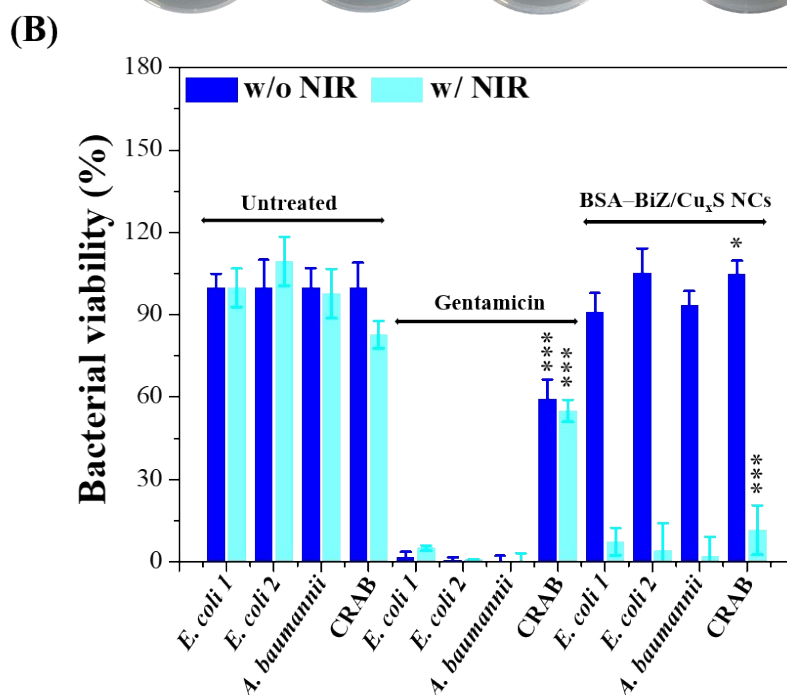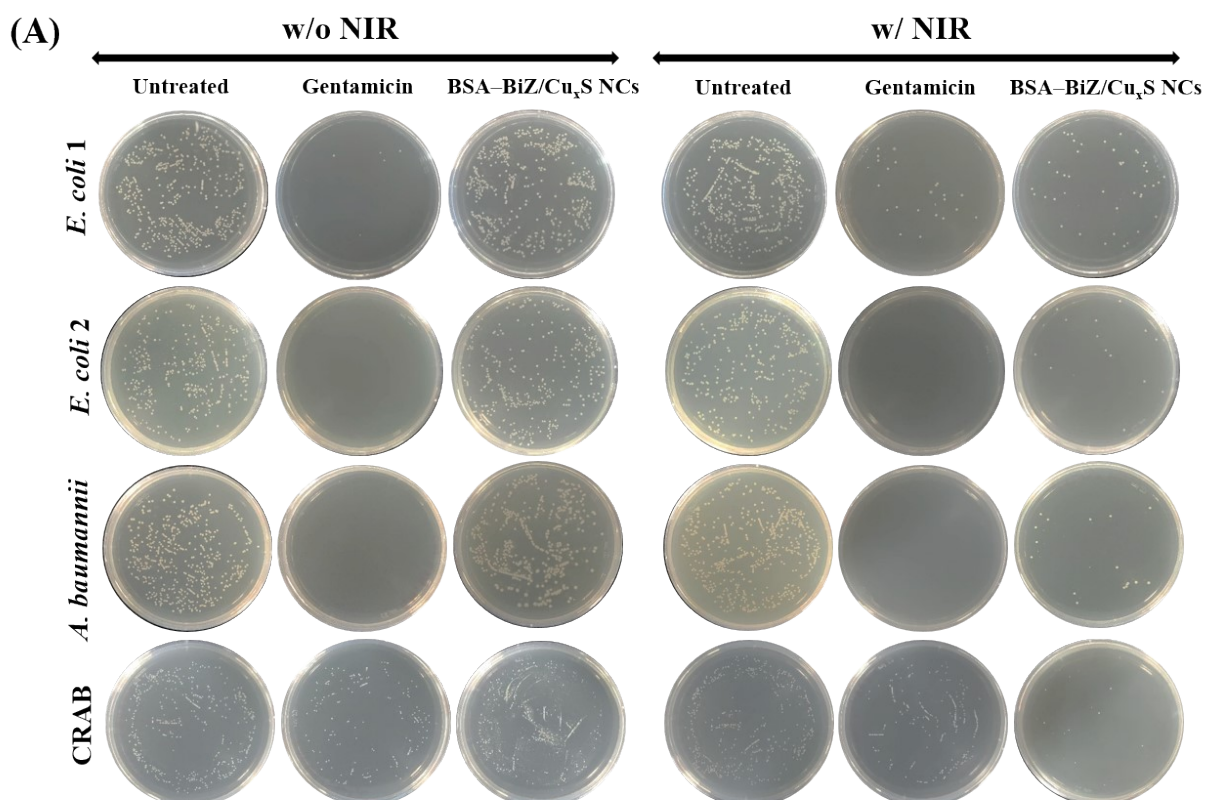
Fig. S14. (A) Representative colony formation and (B) bacterial viability of Gram-negative clinical isolates untreated and treated with gentamicin (100 μg mL^{-1}) or BSA–BiZ/Cu$_x$S NCs ([Cu] = 4.0 μg mL^{-1}) dispersed in 10 mM sodium phosphate buffer (pH 7.4) in absence and presence of NIR laser irradiation (808 nm, 0.53 W cm^{-2}) for 10 min. Error bars in (B), represent the standard deviation of three repeated measurements. Asterisks indicate statistically significant differences of the gentamicin and BSA–BiZ/Cu$_x$S NCs treated *S. epidermidis* groups as compared to the untreated ones w NIR and w/o NIR, respectively (*p < 0.05, **p < 0.005, and ***p < 0.001).
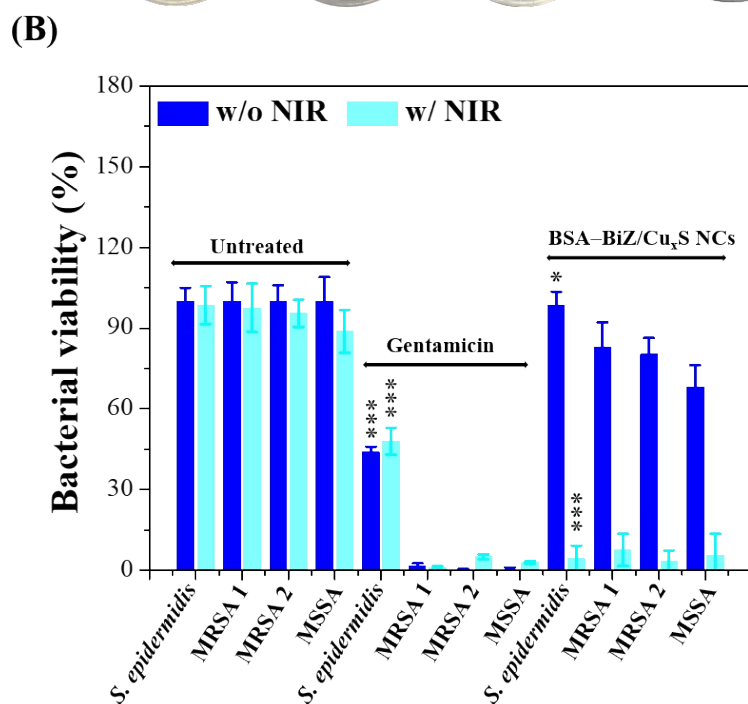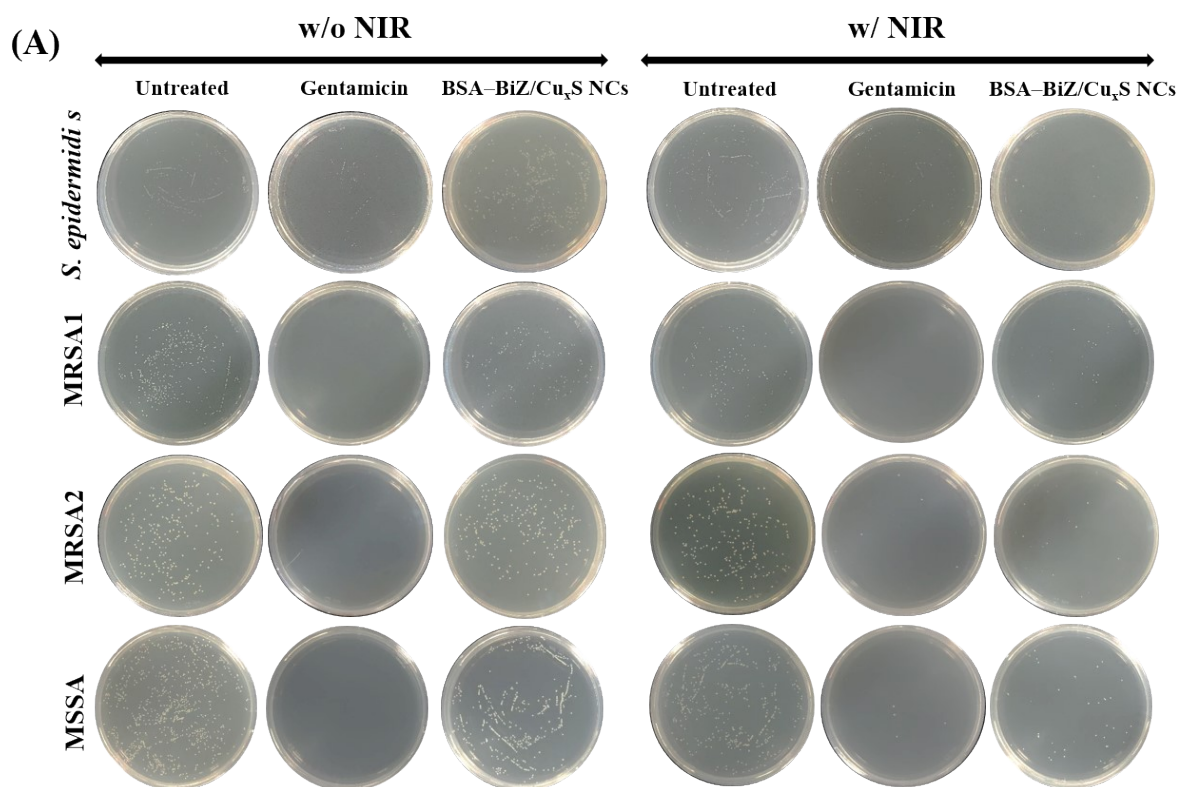
Fig. S15. (A) Representative colony formation and (B) bacterial viability of Gram-positive clinical isolates untreated and treated separately with gentamicin (100 µg mL^{-1}) and BSA–BiZ/Cu$_x$S NCs ([Cu] = 4.0 µg mL^{-1}) dispersed in 10 mM sodium phosphate buffer (pH 7.4) in absence and presence of NIR laser irradiation (808 nm, 0.53 W cm^{-2}) for 10 min. Error bars in (B), represent the standard deviation of three repeated measurements. Asterisks indicate statistically significant differences of the gentamicin and BSA–BiZ/Cu$_x$S NCs treated *S. epidermidis* groups as compared to the untreated ones w NIR and w/o NIR, respectively (*p < 0.05, **p < 0.005, and ***p < 0.001).
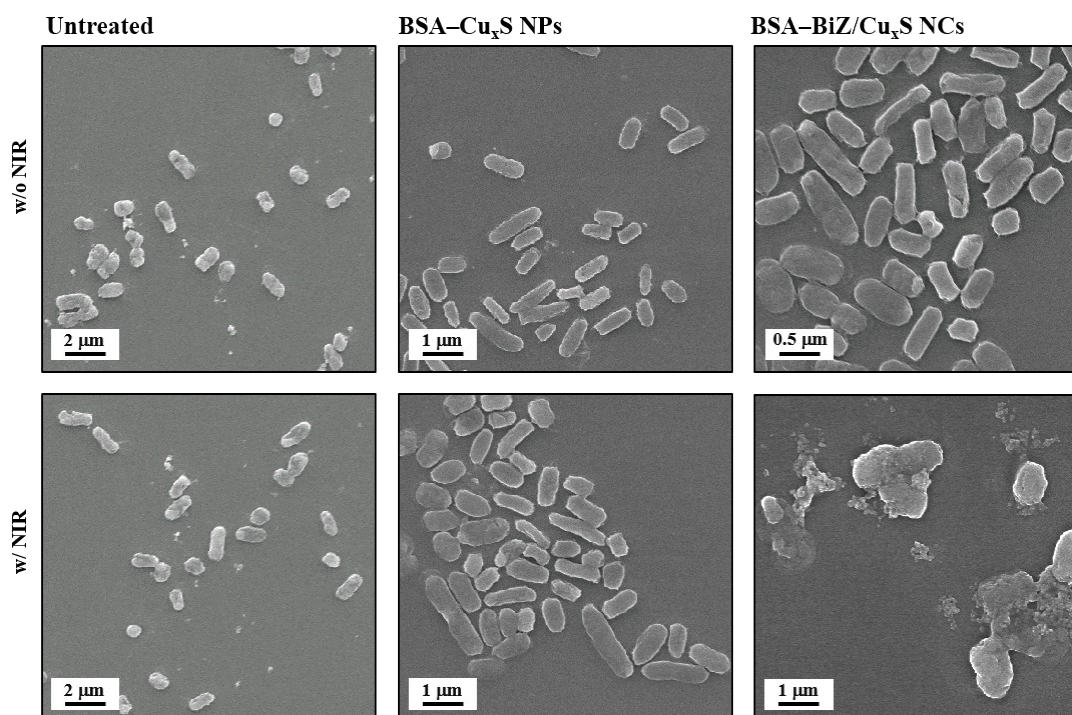
	Untreated	BSA–Cu$_x$S NPs	BSA–BiZ/Cu$_x$S NCs

w/o NIR — 2 µm — 1 µm — 0.5 µm

w/ NIR — 2 µm — 1 µm — 1 µm

Fig. S16. SEM images of *E. coli* (1.0×10^4 CFU mL^{-1}) untreated and separately treated with 4.0 µg mL^{-1} (in terms of Cu) of BSA–BiZ/Cu$_x$S NCs and BSA–Cu$_x$S NPs without or with NIR laser irradiation (808 nm, 0.53 W cm^{-2}) for 10 min.
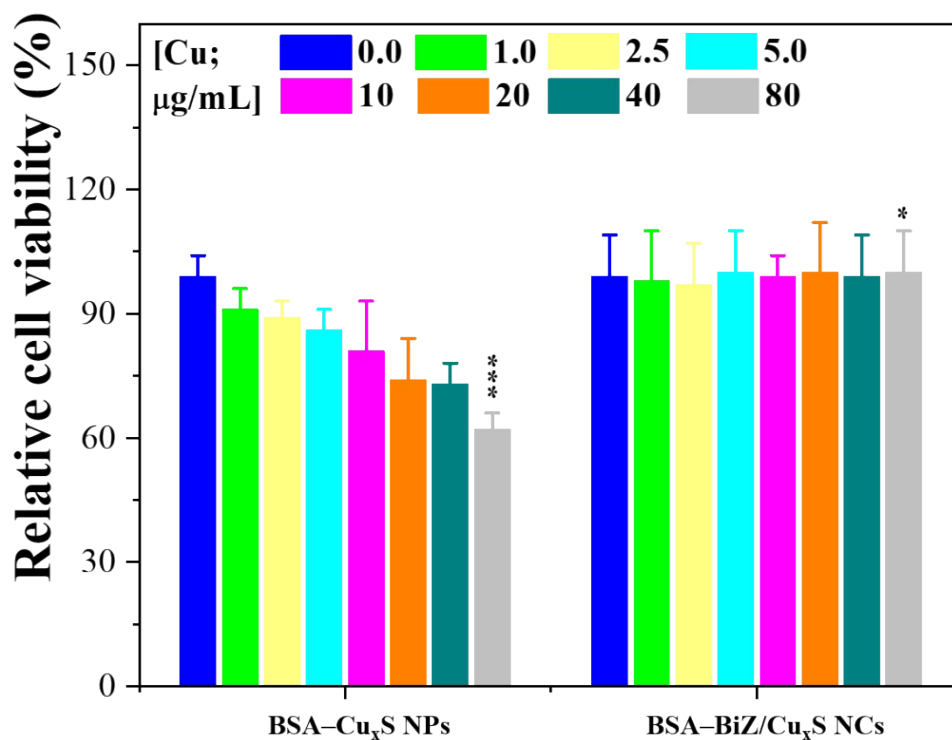
Fig. S17. Relative cell viability of HaCaT (1.0×10^4 cells well^{-1}) after separate incubation with various concentrations (in terms of Cu) of BSA–BiZ/Cu$_x$S NCs and BSA–Cu$_x$S NPs in DMEM containing 10% FBS for 48 h at 37 °C. The error bars represent the standard deviation of four repeated measurements. Asterisks indicate statistically significant differences of the BSA–Cu$_x$S NPs and BSA–BiZ/Cu$_x$S NCs treated groups (80 µg mL^{-1}) as compared to the untreated ones (0.0 µg mL^{-1}) (*$p < 0.05$, **$p < 0.005$, and ***$p < 0.001$).
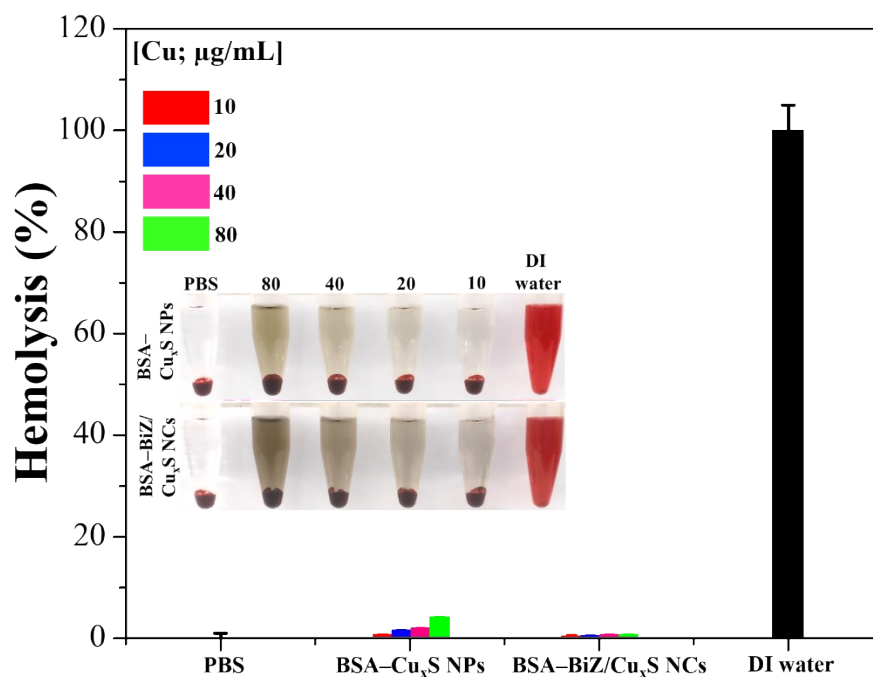
Fig. S18. Hemolytic activities of BSA–BiZ/Cu$_x$S NCs and BSA–Cu$_x$S NPs dispersed in PBS solution against RBCs. The RBCs treated with PBS and DI water served as negative and positive controls, respectively. Insets: photographs of RBCs (4% v/v) after incubation in PBS, DI water or various concentrations (in terms of Cu) of BSA–Bi/Cu$_x$S NCs or BSA–Cu$_x$S NPs. The error bars represent the standard deviation of four repeated measurements.
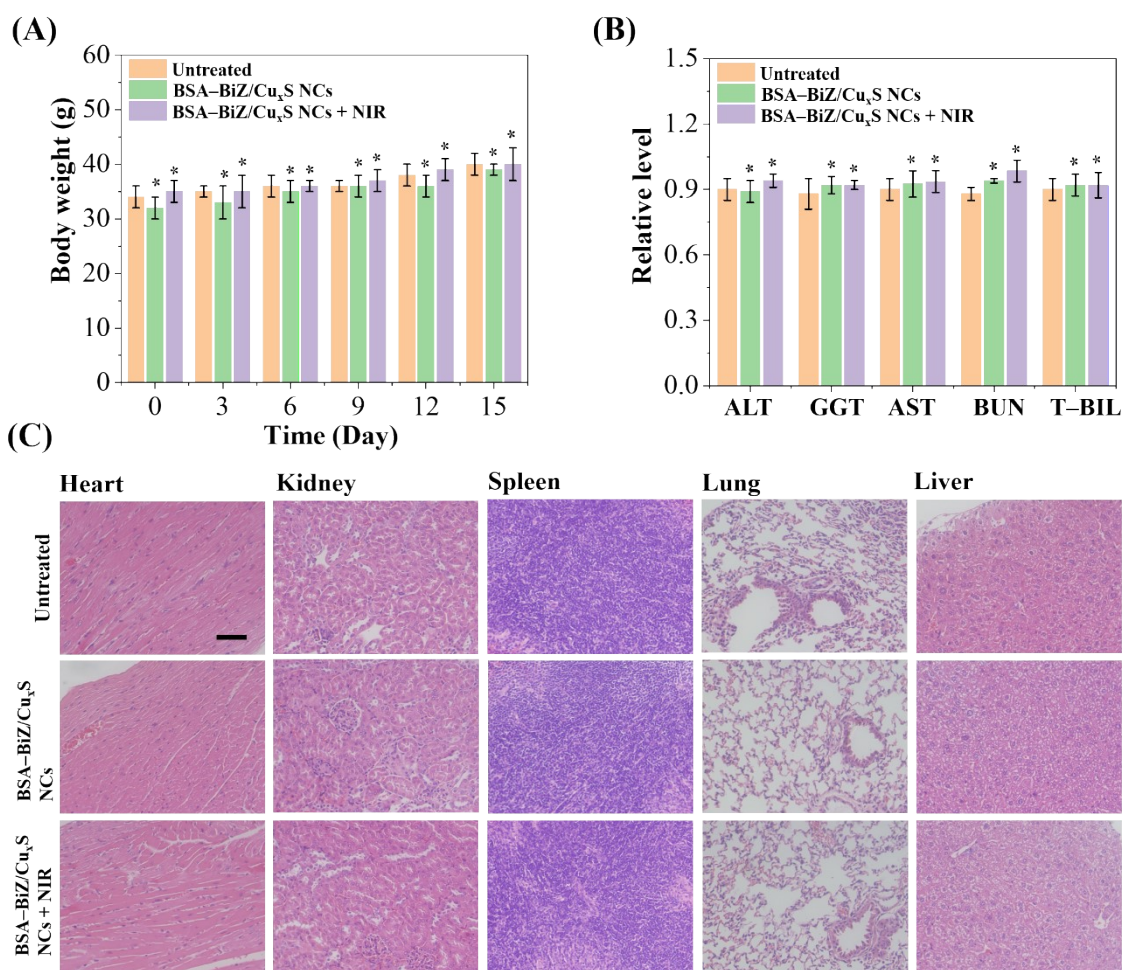
Fig. S19. (A) Body weight of untreated and treated mice with BSA–BiZ/Cu$_x$S NCs for 15 days. (B) Relative levels of ALT, GGT, AST, BUN , and T–BIL in the blood stream of mice before and after administration of BSA–BiZ/Cu$_x$S NCs for 15 days. (C) H&E staining of the tissues excised (thickness~6 μm) at day 15 post treatment. Scale bar is 100 μm. Error bars in (A) and (B) shows the standard deviation of three repated measurements. Asterisks indicate statistically significant differences of the BSA–BiZ/Cu$_x$S NCs treated groups (w/ NIR and w/o NIR) as compared to the untreated ones (*$p < 0.05$, **$p < 0.005$, and ***$p < 0.001$).

Table S1. Atomic compositions of BSA–BiZ/Cu$_x$S NCs, BSA–Cu$_x$S NPs, and BSA–Bi$_2$S$_3$ NPs estimated by elemental analysis and ICP-MS.

Nanomaterials	O (%)[a]	S (%)[a]	Cu (%)[a]	Bi (%)[a]
BSA–BiZ/Cu$_x$S NCs	17.5±0.05	23.3±0.06	26.7±1.10	14.2±0.06
BSA–Cu$_x$S NPs	19±1.81	16.7±0.83	52.6±1.5	ND[b]
BSA–Bi$_2$S$_3$ NPs	26.4±0.13	7.0±0.05	ND[b]	16.1±0.12

[a]error bars represent standard deviations from four repeated experiments; [b]not detected

Reference:

1 Q. Guo, F. Liang, Z. Sun, Y. Wang, X. B. Li, S. G. Xia, Z. C. Zhang, L. Huang, L. Z. Wu, *J. Mater. Chem*. *A*, 2020, **8**, 22601.